Mon. Not. R. Astron. Soc. **000**, 000–000 (0000) Printed 7 October 2009 (MN LATEX style file v2.2)

Optimizing baryon acoustic oscillation surveys II: curvature, redshifts, and external datasets

David Parkinson⋆[1], Martin Kunz,[1] Andrew R. Liddle[1], Bruce A. Bassett[2,3], Robert C. Nichol[4] and Mihran Vardanyan[5]

[1] *Astronomy Centre, University of Sussex, Brighton, BN1 9QH, U.K.*
[2] *South African Astronomical Observatory, P.O. Box 9, Observatory 7935, Cape Town, South Africa*
[3] *Department of Maths and Applied Maths, University of Cape Town, South Africa*
[4] *Institute of Cosmology & Gravitation, University of Portsmouth, Portsmouth, P01 2EG, U.K.*
[5] *Astrophysics Department, University of Oxford, Denys Wilkinson Building, Keble Road, Oxford, OX1 3RH, U.K.*

7 October 2009

ABSTRACT

We extend our study of the optimization of large baryon acoustic oscillation (BAO) surveys to return the best constraints on the dark energy, building on Paper I of this series (Parkinson et al. 2007). The survey galaxies are assumed to be pre-selected active, star-forming galaxies observed by their line emission with a constant number density across the redshift bin. Star-forming galaxies have a redshift desert in the region $1.6 < z < 2$, and so this redshift range was excluded from the analysis. We use the Seo & Eisenstein (2007) fitting formula for the accuracies of the BAO measurements, using only the information for the oscillatory part of the power spectrum as distance and expansion rate rulers. We go beyond our earlier analysis by examining the effect of including curvature on the optimal survey configuration and updating the expected 'prior' constraints from Planck and SDSS. We once again find that the optimal survey strategy involves minimizing the exposure time and maximizing the survey area (within the instrumental constraints), and that all time should be spent observing in the low-redshift range ($z < 1.6$) rather than beyond the redshift desert, $z > 2$. We find that when assuming a flat universe the optimal survey makes measurements in the redshift range $0.1 < z < 0.7$, but that including curvature as a nuisance parameter requires us to push the maximum redshift to 1.35, to remove the degeneracy between curvature and evolving dark energy. The inclusion of expected other data sets (such as WiggleZ, BOSS and a stage III SN-Ia survey) removes the necessity of measurements below redshift 0.9, and pushes the maximum redshift up to 1.5. We discuss considerations in determining the best survey strategy in light of uncertainty in the true underlying cosmological model.

Key words: cosmological parameters – large-scale structure of universe – surveys

1 INTRODUCTION

The discovery of the accelerating universe, driven by some mysterious dark energy, has motivated the conceptualization and design of a number of future surveys that will seek to discover its nature. These include, but are not limited to: Wide-field Fiber-fed Multi-Object Spectrograph (WFMOS), the Dark Energy Survey (DES), Panoramic Survey Telescope & Rapid Response System (Pan-STARRS), Baryon Oscillation Spectroscopic Survey (BOSS), Large Sky Area Multi-Object Fibre Spectroscopic Telescope (LAMOST), Hubble Sphere Hydrogen Survey (HSHS), Square Kilometre Array (SKA), Large Synoptic Survey Telescope (LSST), Euclid and the Joint Dark Energy Mission (JDEM). These will deploy an array of methods to probe the dark energy, such as baryon acoustic oscillations (BAO), weak lensing, cluster number counts, and type-Ia supernovae (SN-Ia).

In such a crowded marketplace it is important to have a compelling product by demonstrating effective use of resources. In previous papers some of the present authors have examined the application of design principles to the construction of new surveys, by optimizing the surveys to give the best science return (Bassett 2005; Bassett, Parkinson & Nichol 2005a). Also, recently a team commissioned by the

⋆ drp21@sussex.ac.uk

US NSF (the Dark Energy Task Force or DETF) laid out a 'roadmap' of how dark energy experiments may develop into the future (Albrecht et al. 2006), and similar studies have been undertaken by UK and European funding agencies.

This paper is a continuation of our previous work (Parkinson et al. 2007, hereafter P07), in which we considered optimizing a BAO survey similar to the WFMOS design.[1] The conceptual design for the WFMOS dark energy survey is to conduct a large area survey of the sky, measuring the redshifts of order millions of galaxies. The power spectrum of these galaxies traces the power spectrum of the underlying matter density, and this contains the imprint of the primordial sound waves in the photon–baryon plasma (the BAO). These 'wiggles' in the power spectrum can be used as standard rulers to measure the angular-diameter distance ($d_{\rm A}$) from those modes transverse to the line of sight, and the Hubble rate at that redshift ($H(z)$) from the radial modes. For a description of WFMOS, see Bassett, Nichol & Eisenstein (2005b). Very similar surveys have been proposed for LAMOST (Wang et al. 2009) and the 4-m Mayall telescope (BigBOSS; Schlegel et al. 2009b).

In P07 we set out the basics of our optimization methodology, defining the concepts of a Figure of Merit (FoM), very similar to the one proposed by the DETF but now as a function of survey strategy, and a survey parameter space, where a particular survey configuration is defined in terms of time, area and redshift. When these survey parameters are combined with information about the instrument, we can predict the number of galaxies that will be observed, the accuracy with which the BAO will be measured, and the resulting FoM. By plotting how the FoM varies with survey parameters, we can find the optimal survey. We found that the optimization preferred the surveys to be as large in area as possible, limiting the exposure time to be as small as possible, to beat down the shot noise from limited galaxy numbers.

In this paper we address the issues of the survey redshift ranges in the high and low-redshift regimes, and the time spent observing in each of them. We see how these survey parameters are affected by the cosmological parameters being considered, and by the other surveys that are included as priors in the analysis.

In Section 2 we briefly review the details of our previous optimization, before describing the details of how our analysis has been updated. In Section 3 we state the optimal configurations for a WFMOS-like survey by itself. In Section 4 we look at the effect on the optimal survey design of adding in other experimental data as 'prior' measurements. In Section 5 we outline our conclusions.

2 OPTIMIZATION PROCEDURE

2.1 Survey definition

We perform our optimization as described in P07. We consider a set of allowed survey geometries, described by the parameters listed in Table 1, and illustrated by a schematic in Figure 1. A general survey is divided into low- and high-redshift components, the former corresponding to $z < 1.6$ and the latter $z > 2$, separated by the redshift desert within which ground-based surveys cannot effectively obtain redshifts due to the lack of galaxies emitting in the optical wavelengths. The terminology 'low' and 'high' has this meaning throughout.

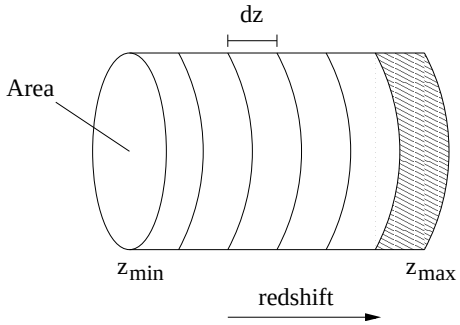

Figure 1. A schematic illustrating how the survey parameters are defined. The survey volume is defined by the area on the sky and the minimum and maximum redshifts. The redshift range is subdivided into a number of slices of fixed width dz for computing the FoM. The number density is fixed by the density in the final redshift slice (the shaded region) for a given exposure time.

Table 1. List of survey parameters in each redshift regime. See Parkinson et al. (2007) for detailed explanations. Note that we no longer vary the number of redshift bins, but instead divide up the redshift ranges into thin slices for the FoM calculation.

Survey Parameter	Symbol
Survey time	$\tau_{\rm low}$, $\tau_{\rm high}$
Area covered	$A_{\rm low}$, $A_{\rm high}$
Minimum of redshift bin	$z_{\rm low}$ (min), $z_{\rm high}$ (min)
Maximum of redshift bin	$z_{\rm low}$ (max), $z_{\rm high}$ (max)
Number of pointings	$n_{\rm p}$(low), $n_{\rm p}$(high)

The survey parameters are limited by some constraints, listed in Table 2. These are the same as in P07, with the exception of the limits on the redshift bins ($z_{\rm min}$, $z_{\rm max}$), which have been relaxed as we now include a more reasonable model of the efficiency/response of the WFMOS spectrograph to light at different wavelengths. The details of this wavelength throughput are not public, but can be taken to be very similar to that of the Sloan Digital Sky Survey (SDSS) spectrographs.[2]

Having established the details of the survey, we compute the total number of galaxies that will be measured. We assume a pre-existing source catalogue of photometrically selected galaxies, from which we can effectively target either line-emission active star-forming galaxies or passively-evolving continuum emission galaxies. These details have not changed from the previous paper. Since we found in P07 that the active star-forming galaxies, whose redshifts are to be obtained by measuring the O[II] emission line doublet at

[1] As of May 2009 the original WFMOS project has been terminated through lack of sufficient available funding via the Gemini Observatory, but our methodology and qualitative conclusions are generally applicable to any similar future proposals.

[2] Details of the SDSS spectrographs can be found at http://www.astro.princeton.edu/PBOOK/spectro/spectro.htm

Table 2. List of constraint parameters.

Constraint Parameter	Value
Total observing time	1500 hours
Field of view	1.5^o diameter
$n_{\rm fibres}$	3000
Aperture	8m
Fibre diameter	1 arcsec
Overhead time between exposures	10 mins
Minimum exposure time	15 mins
Maximum exposure time	10 hours
Wavelength response	Priv. comm with AAO
Width of redshift slices, dz	0.05

low redshift and Lyman-α at high redshift, are the preferred targets, we adopt these as standard for all the analysis in this paper. We also set a somewhat arbitrary lower limit of 15 minutes for the exposure time, representing a reasonable compromise when taking into account a rather pessimistic estimate of a 10 minute overhead time between exposures. We further assume that the galaxies are targeted so as to generate a sample of uniform number density across each redshift bin.

We also include an estimate of the bias of these galaxies, and its evolution with redshift. At low redshift we take Wake et al. (2008) as our guide, assuming the bias (weakly) tracks the linear growth function, using the following formula

$$b(z_{lo}) = 1 + (b(z_{hi} - 1)D(z_{hi})/D(z_{lo})\,, \qquad (1)$$

where $D(z0$ is the growth function. Here we take $z_{hi} = 0.55$ and $b(z_{hi}) = 1.3$ At high redshift we use the result of Myers et al. (2007) that the bias grows as $(1 + z)^2$.

Once the redshift ranges and number of galaxies have been determined, the cosmological parameter analysis can proceed. Here we slice the redshift bins into a number of sub-bins, where the width of these sub-bins is fixed and the number is determined by the redshift range (as shown in Figure 1). We take the width of the redshift slices to be constant, $dz = 0.05$, with the redshift range always being an integer number of these slices and the minimum and maximum redshifts discretized in the same units.

In computing the BAO errors on each slice, we do not include the possible correlations between slices that may be caused by large-scale modes in the power spectrum. Our slice width dz is chosen to be fairly wide to reduce such correlations. These will have the effect of decreasing the constraining power of the survey and so lowering the FoM. We do not necessarily expect including these effects to change the optimal survey, as they will not change the redshifts at which the measurements are being made, only the accuracy of the measurements.

2.2 Figure of Merit (FoM)

Once the area, redshift range and slices, and galaxy number of the survey have been determined, we can use fitting formulae to estimate how well the BAO will be measured, and what distance information will be returned. In Rassat et al. (2008) a comparison was made between different methods for extracting information from a future galaxy survey. Here, following on from P07, we only use the oscillatory part of the power spectrum (the 'wiggles'), as we consider this the most robust source of distance information that can be extracted. The full power spectrum is degenerate with primordial power spectrum parameters (tilt, running) and also details of the growth of structure on large scales (non-linear bias, non-linear growth). The anisotropy of the power spectrum can be used as an Alcock–Paczynski (AP) test, but this require details of the non-linear behavior of the redshift-space distortions.

In P07 we used the formula published by Blake et al. (2006), but this has been superseded by those of Seo & Eisenstein (2007). We use the formula derived from a Fisher matrix approach, using a 2-D approximation of only the oscillatory part of the power spectrum (equation 26 in their paper). These fitting formula estimate the errors in the position of the baryonic features along and across the line of sight, as well as the correlation between them. They also have the added advantage that they can simulate the effect of 'reconstruction' of the linear oscillations in the non-linear regime (though we do not use reconstruction in this paper). This can lead to increased accuracy at lower redshifts, where non-linear effects on the power spectra are present at the same scales as the BAO. The accuracies of the BAO measurements leads to the calculation of the FoM.

In P07, as in the DETF report, the CPL parameterization (Chevallier & Polarski 2001; Linder 2003) of the dark energy equation of state was used, given by

$$w(a) = w_0 + w_a(1 - a)\,, \qquad (2)$$

where w_0 and w_a are adjustable constants. The FoM we used in the previous paper was the D-optimal criterion, the inverse of the determinant of the (w_0, w_a) covariance matrix, i.e.

$$\mathrm{FoM_{old}} = \det{}^{-1}(\mathbf{C}) = \frac{1}{\sigma^2_{w_0 w_0}\sigma^2_{w_a w_a} - \sigma^4_{w_0 w_a}} \qquad (3)$$

Here we have switched to the square root of the inverse of the determinant, bringing us into line with the DETF FoM,

$$\mathrm{FoM_{new}} = \frac{1}{(\sigma_{w_a}\sigma_{w_{\rm p}})} = \frac{1}{\sqrt{\sigma^2_{w_0 w_0}\sigma^2_{w_a w_a} - \sigma^4_{w_0 w_a}}}\,, \qquad (4)$$

where $w_{\rm p}$ is the equation of state at the 'pivot' redshift. Hence our new FoM is the square root of our old FoM. We use this new definition of the FoM throughout.

The FoM is computed using a Fisher matrix approach. Details are laid out in Appendix A.

2.3 Adding curvature

We have expanded our cosmological parameter space from P07, by including the effect of curvature on our analysis. The importance of doing so has been emphasized by Clarkson, Cortes & Bassett (2007), who showed than even a small curvature can seriously bias dark energy measurements. Our cosmological parameter space (Θ) is now defined to be

$$\Theta = \{w_0, w_a, \Omega_{\rm DE}, \Omega_k, h, \Omega_{\rm b}h^2, n_{\rm s}\}\,. \qquad (5)$$

The fiducial values for these parameters are given in Table 3. Additional parameters not allowed to vary are the radiation energy density $\Omega_{\rm r}$ and the matter spectrum normalization σ_8. Note that the 'wiggles-only' method of BAO does not

Table 3. The fiducial cosmological parameters used in this paper.

Parameter	Value
w_0	-1
w_a	0
$\Omega_{\rm m}$	0.3
$\Omega_{\rm r}$	8.2×10^{-5}
Ω_k	0
$\Omega_{\rm DE}$	$1 - \Omega_k - \Omega_{\rm m} - \Omega_{\rm r}$
H_0	70
$\Omega_{\rm b}$	0.0441
$n_{\rm s}$	1
σ_8	0.9

constrain σ_8 directly, it is included here as it is an input parameter into the Seo & Eisenstein (2007) fitting formula.

We include the measurements of the BAO by SDSS and 2dF (Eisenstein et al. 2005, Percival et al. 2007) as prior information. The SDSS/2dF prior is the ratio of measurements of $D_{\rm V}$ at $z = 0.2$ and $z = 0.35$, where D_V is defined as

$$D_V \equiv [r^2 cz/H(z)]^{1/3} \,. \tag{6}$$

The accuracy of this measurement is given in Percival et al. (2007).

We also include measurements of the CMB by the Planck satellite (Mukherjee et al. 2008) as prior information. Planck will make accurate measurements of the distance to last scattering (R) and the position of the first peak (l_a), defined to be

$$R \equiv \sqrt{\Omega_{\rm m} H_0^2}\, r(z_{\rm CMB}) \,, \quad l_a \equiv \frac{\pi r(z_{\rm CMB})}{r_s(z_{\rm CMB})} \,. \tag{7}$$

The accuracy of these measurements was estimated by simulating temperature and polarisation power spectra (i.e. using TT, TE and EE), and running Markov Chain Monte Carlo (MCMC) chains to estimate the error on R and l_a, as described in Mukherjee et al. (2008). The results of this paper requires us to include $\Omega_{\rm b}h^2$ and n_s in our analysis.[3] We model the predicted Planck likelihood using the covariance matrix on these four parameters (R, l_a, $\Omega_{\rm b}h^2$ and n_s) given in Mukherjee et al. (2008). Note that the constraints on $\Omega_{\rm b}h^2$ and n_s only come from the CMB, and these parameters would not be constrained by BAOs only. There is a loss of information in considering only the constraints on these four parameters rather than the full CMB power spectra, but Mukherjee et al. (2008) found that when considering constraints on Dark Energy models and combining this condensed form of information with other distance probes this information loss is negligible.

2.4 Searching the parameter space

We search through the survey parameter space as in P07 using simulated annealing, with long MCMC chains undergoing thermodynamic scheduling (see Cerny 1985) to push them closer to the optimum. The FoM takes on the role of the likelihood in parameter estimation MCMC, where the probability of moving from a survey configuration (s) to a new one (s') is given by

$$P(s \to s') = \min\left\{1, \frac{\mathrm{FoM}(s')}{\mathrm{FoM}(s)}\right\} \,. \tag{8}$$

By employing thermodynamic scheduling, we introduce a temperature T that modulates the probability of acceptance, thus

$$P(s \to s') = \min\left\{1, \left(\frac{\mathrm{FoM}(s')}{\mathrm{FoM}(s)}\right)^{1/T}\right\} \,. \tag{9}$$

As the temperature of the chain goes from 'hot' to 'cold' the probability of accepting a survey with a smaller FoM rapidly diminishes. This technique is employed for example in Wit, Nobile & Khanin (2005), and has also been used in optimizing cluster surveys for probing the Dark Energy in Wu, Rozo & Wechsler (2009), which appeared after this paper.

The nature of optimization is that we are interested only in a tiny region of the survey parameter space, and so large numbers of chain elements are not necessarily a guarantee of reaching the true global optimum. Some of the parameters we have included may have only small contributions to the FoM, or may actually be detrimental (e.g. observing at high redshift may reduce the FoM as it reduces the time that can be spent observing at low redshift). We therefore often run refinement searches, in a lower-dimensional parameter space, to speed up reaching the optimum. When the MCMC search indicates that some of the parameters (time spent at high redshift, exposure time etc) can be set to specific values, a follow-up search is carried out with these parameters fixed to refine the optimal survey.

One aim of the optimization is to discover how far we can push the survey away from the optimum configuration without degrading the performance too much. For this we introduce 'flexibility bounds', which describe or delimit the region of parameter space where the FoM has fallen to 90% and 60% of the optimum value. This idea was introduced in P07, but as we have changed our definition of FoM from that paper, we have also changed our definition of the flexibility bounds in line with that. The flexibility bounds are interesting as they show the relationship between survey parameters, such as the survey area and time.

2.5 Effect of methodology changes from Paper I

As compared to P07, this paper makes significant changes to the methodology. On the observational side is an improved understanding of the WFMOS instrument, the adoption of the BAO fitting formulae of Seo & Eisenstein (2007), and the improvement of prior information from SDSS and expected from Planck. On the theoretical side is the inclusion of curvature within the cosmological model. To illustrate the effect of these changes, we consider a 'standard', non-optimized, WFMOS survey outlined in Table 4. This is intended to represent the sort of survey assumptions one might have made without optimizing. We compare three different calculations of the FoM.

Under the old methodology, with a flat Universe, the FoM was 7. Improved understanding of the instrument and

[3] We could have included a prior from Big Bang Nucleosynthesis, which yields $\Omega_{\rm b}h^2 = 0.0214 \pm 0.0020$. However, Planck will constrain $\Omega_{\rm b}h^2$ well enough that such a prior has a minuscule effect on the FoM, changing only the 4^{th} decimal place.

Table 4. Survey parameters and FoMs for a 'standard' (non-optimized) survey (including Planck and SDSS as prior information).

Survey Parameter	Value
$A_{\rm low}$ (sq. degrees)	2000
$\tau_{\rm low}$ (hours)	800
$z_{\rm low}$ (min)	0.5
$z_{\rm low}$ (max)	1.3
exposure time (minutes)	32
number density (Mpc$^{-3}h^3$)	8.3×10^{-4}
number of galaxies	3.4×10^6
$A_{\rm high}$ (sq. degrees)	300
$\tau_{\rm high}$ (hours)	700
$z_{\rm high}$ (min)	2.3
$z_{\rm high}$ (max)	3.3
exposure time (minutes)	237
number density (Mpc$^{-3}h^3$)	4.5×10^{-4}
number of galaxies	5.5×10^4
FoM (old method, flat Universe)	7
FoM (new method, flat Universe)	18
FoM (new method, with curvature)	9

additional prior information has indicated that it will be significantly more powerful; under the same flat Universe assumption the FoM is improved to 18, substantially reducing the uncertainty of each of the two dark energy parameters. Inclusion of curvature, however, necessarily degrades the outcome, lowering the FoM to 9.

3 WFMOS OPTIMAL SURVEYS

We break the results of the analysis down into the following subsections. In Section 3.1 we review the results from our previous work, then in Section 3.2 we look at the effect of adding curvature on the time split between the two redshift regimes. In Section 3.3 we discuss the best survey strategy in light of uncertainty in the true underlying cosmological model. In this section we only assume priors from SDSS and Planck.

It would be possible to do an optimization for the experiment without any prior information, but it would be misleading to carry out such an optimization. The SDSS data already exists, and the Planck data will do soon (and even WMAP measurements might be good enough for this purpose) and the principal goal of optimization is to find the correct niche for an experiment. If a survey such as WFMOS were forced to spend time observing at high redshift to remove the degeneracy with curvature, when it could just as easily do so by incorporating the results from Planck, this would be waste of time and resources, and the incorrect kind of optimization to perform. It is therefore imperative to account for all relevant information already available when optimizing a future survey.

3.1 Previous work

In our previous paper we conducted an analysis where we varied only four parameters (w_0, w_a, $\Omega_{\rm m}$ and $\Omega_{\rm m}h^2$), assuming the Universe to be flat so the dark energy density is given by $\Omega_{\rm DE} = 1 - \Omega_{\rm m}$. We found that the optimization preferred to concentrate all the survey time into the low-redshift regime. We also found that short exposure times of just a few minutes on an 8-metre class telescope are sufficient to obtain redshifts for the majority of line-emission galaxies. Although a longer exposure time would result in higher quality spectra with fewer wasted fibres, it also reduces the amount of area that can be surveyed during a fixed total survey duration. A large area is important to maximize the number of surveyed galaxies, so that the shot noise can be beaten down. The optimal surveys were therefore driven to the smallest allowed exposure time of 15 minutes. The best strategy was to ignore the possibility of high-redshift observations, as there were no parameter degeneracies that required such observations to break them.

Table 5. Optimal survey parameters, optimized for a flat universe and including curvature as a nuisance parameter. The FoM is computed including prior information from Planck and SDSS, as described in the text. The parameters for the high redshift bin are not included as the optimal surveys spend all their time observing at low redshift. We also include the one sigma errors on the cosmological parameters predicted by the Fisher matrix approach for these optimal surveys.

Survey Parameter	Flat	Curved
$A_{\rm low}$ (sq. degs)	6300	6300
$\tau_{\rm low}$ (hours)	1500	1500
$z_{\rm low}$ (min)	0.1	0.1
$z_{\rm low}$ (max)	0.7	1.35
exposure time (mins)	15.0	15.0
number density (h^3/Mpc^3)	3×10^{-3}	6.6×10^{-4}
number of galaxies	10.8×10^6	10.8×10^6
FoM	57	32
$\sigma(w_0)$	0.14	0.23
$\sigma(w_a)$	0.44	0.70
$\sigma(\Omega_{\rm DE})$	0.012	0.018
$\sigma(\Omega_k)$	-	2.5×10^{-3}

We reanalyzed this case, taking into account all the improvements we had made, but still assuming a flat universe where the curvature is not included as a nuisance parameter in the calculation of the FoM. We recovered very similar results to those given in P07. The optimal survey parameters are given in Table 5, and the FoM as a function of the survey parameters (for the low-redshift bin only) is shown in Figure 2. The detailed results of this analysis are shown in Figure B1 in Appendix B.

The optimized survey represented a substantial gain in FoM with respect to the 'standard' survey.

3.2 Adding curvature as a parameter

We now want to understand the effect of including the curvature of the Universe Ω_k as a free parameter in our analysis on the best survey. We continue to assume a flat fiducial cosmology, but now require our observations to also constrain curvature.

In Table 5 we show the optimal survey allowing for curvature as a nuisance parameter. We see that the optimal FoM is reduced, as the inclusion of an extra parameter (Ω_k) degrades the constraints on w_0, w_a. We find once again that

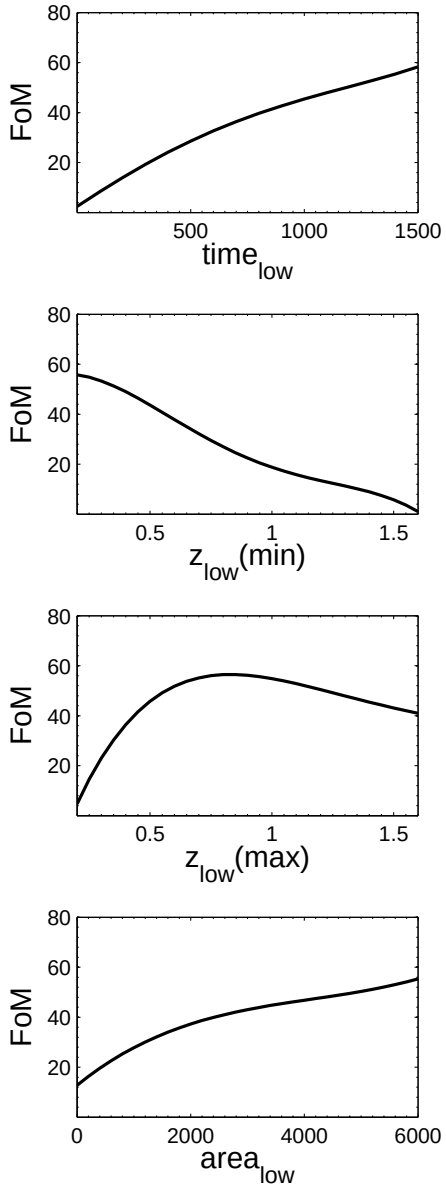

Figure 2. The FoM as a function of the survey parameters, where the surveys have been optimized assuming a flat universe. The other parameters were chosen to maximize the FoM. The area and redshifts of the high-redshift bin have been omitted, as the optimal survey spends all its time observing at low-redshift.

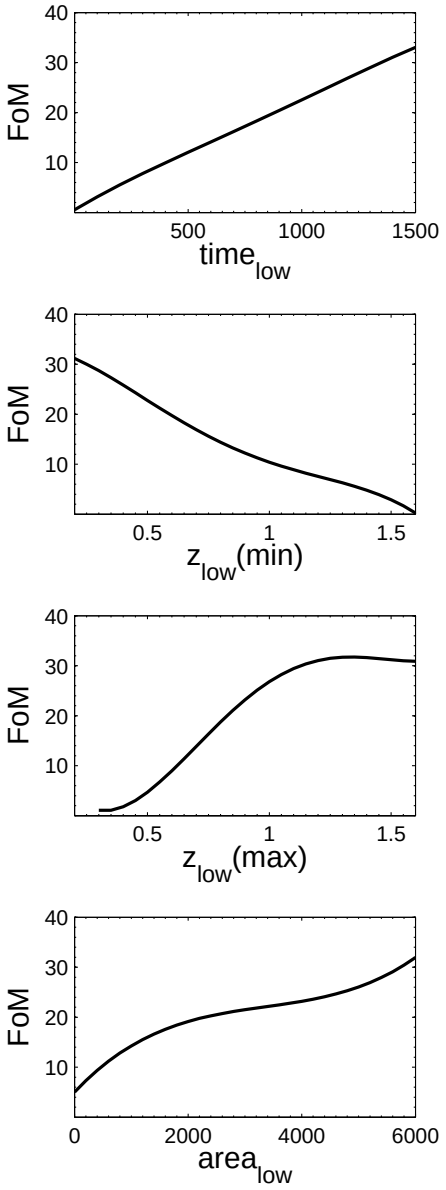

Figure 3. The FoM as a function of the survey parameters, where the other survey parameters are chose to maximize the FoM. The surveys were optimized including curvature as a nuisance parameter.

the preferred survey is one that spends all its time observing at low redshift. However, in contrast to the flat case, we see that the maximum redshift of the low-redshift bin is forced up to $z = 1.35$. BAO measurements at these higher redshifts are needed to remove the degeneracy between evolving dark energy and curvature.

The FoM as a function of the survey parameters is shown in Figure 3, and the detailed results of this analysis are shown in Figure B2 in Appendix B. The position of the minimum of the redshift bin is unchanged from the flat case $z_{\rm low}(\min) = 0.1$, while the maximum $z_{\rm low}(\max)$ is pushed up to higher redshifts.

3.3 The optimized survey strategy

We begin by noting the significant impact that optimization can have in improving the science return. The FoM of the optimized case including curvature (32, from Table 5) is much larger than the FoM of the standard baseline survey (9 from Table 4). The amount of reduction in the area of the error ellipse is $32/9 \simeq 3.6$, a large factor, and this is illustrated in Figure 4. Put another way, the optimized survey would reach the same dark energy equation of state accuracy as the standard survey after only about one-quarter of the survey time. The reduced accuracy of the standard survey is because it spends time at high redshift which would be more productively spent at low redshift, and its low-redshift exposures are unnecessarily long.

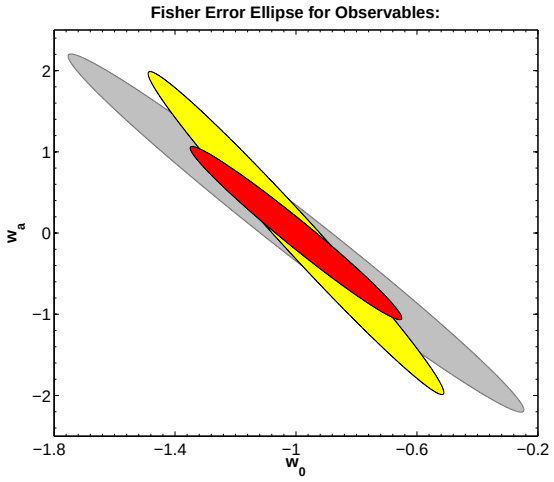

Figure 4. The 68% error ellipse on the w_0 and w_a parameters, with marginalization over curvature, for the standard WFMOS survey (grey), and the optimized one (red). Also shown (yellow) is the error ellipse were the survey optimized for a flat Universe (but the errors have been computed here marginalizing over curvature). The difference between the largest ellipse and the two smaller ones shows the improvement due to optimizing the survey for measuring the dark energy parameters, while the difference between the smaller ellipses is due to different cosmological models (flat or non-flat) used for the optimization. These constraints are calculated including prior information from Planck and SDSS.

Table 6. Optimal survey Figure of Merit calculated in flat and curved cases, where the optimization has been undertaken under two different assumptions, either that Ω_k is left out or included as a nuisance parameter. The FoM in computed including prior information from Planck and SDSS.

Survey optimization	without Ω_k	with Ω_k
FoM (Ω_k set to zero)	57	48
FoM (Ω_k allowed to vary)	15	32

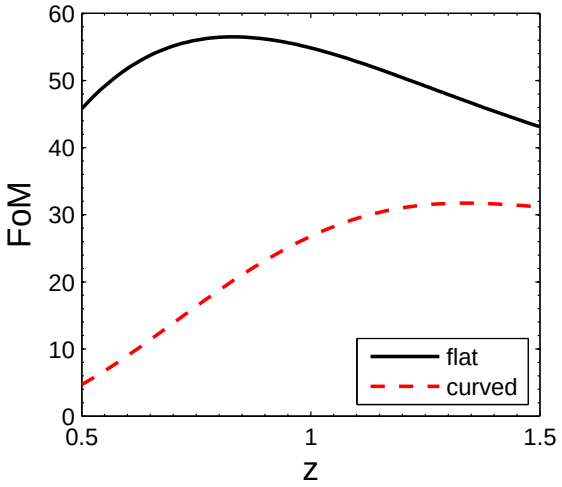

Figure 5. The FoM as a function of the upper redshift limit of the survey, for both the flat case and for the case including curvature. All surveys use $z_{\rm min} = 0.1$ and a minimal exposure time of 15 minutes, as discussed in the text. Measuring the curvature requires targeting a larger redshift range.

Having established the importance of optimization, what considerations determine the optimal survey strategy? The principal uncertainty here is the form of the true cosmological model. This is what we are trying to determine, and there must clearly be competing possibilities for the experiment to be interesting. As the optimal strategy depends on the (unknown) true cosmological model, there will inevitably be choices to be made which have both costs and benefits. In the context of the models considered in this paper, the decision is whether to assume a flat Universe or to allow for curvature; there will be a cost if the assumption made in optimization turns out to be inappropriate once the data are obtained and analyzed.

For the models we have considered here, the basic survey decisions are independent of the assumed cosmological model. The first is that high-redshift observations are unnecessary — all survey time should be spent at low redshift ($z < 1.6$). The second is that the exposures should be as short as possible, as this is already sufficient to obtain the desired redshifts, and hence achieves maximal survey area. Finally, the low-redshift limit can be taken as starting at some suitably low value such as 0.1.

The remaining decision to be made is the upper limit of the low-redshift bin. As we have already seen, the upper redshift limit is different depending whether we assume flatness or not. Table 5 gives the survey parameters for each case.

Table 6 shows the FoMs, now with the extra information of the FoM that is returned if the true cosmology does not match the assumption made in optimizing. Naturally, for a given survey configuration, we get more accurate constraints if we assume a flat Universe than if we allow for curvature, as the extra parameter in the Fisher matrix dilutes the constraining power on dark energy. However, we can now see the losses due to non-optimality. For example, if the Universe really is flat, but we optimized to allow for curvature, our FoM is degraded from 57 to 48. If we end up needing to allow for curvature, having not optimized for it, the degradation is from 32 to 15 (the corresponding error ellipses for this case are shown in Figure 4).

Figure 5 shows the FoMs as a function of the upper redshift limit of the survey (reproduced from Figures 2 and 3), showing the peaks at $z_{\rm max} \sim 0.7$ in the flat case and $z_{\rm max} \sim 1.35$ in the curved one. There is no optimal way to deal with this tension, as one's opinions as to how likely the model assumptions are governs whether the benefits of a particular choice are likely to outweigh the costs. In this particular case existing evidence tends to support a flat Universe (Vardanyan, Trotta & Silk 2009) suggesting that the potential loss of accuracy in the flat case outweighs the ability to measure curvature. If we were considering different dark energy models/parameterizations, the choice may be less clear cut.

Table 7. Best survey parameters when including other data sets. The parameters for the high redshift bin are not included as the optimal surveys spend all their time observing at low redshift. We also include the one sigma errors on the cosmological parameters predicted by the Fisher matrix approach for these optimal surveys.

Survey Parameter	SN-Ia, WiggleZ & BOSS	SN-Ia, WiggleZ & BOSS (+QSO)
$A_{\rm low}$ (sq. degs)	6300	6300
$\tau_{\rm low}$ (hours)	1500	1500
$z_{\rm low}$ (min)	0.9	0.1
$z_{\rm low}$ (max)	1.55	1.6
exposure time (mins)	15.0	15. 0
number density (h^3 Mpc^{-3})	6.7×10^{-4}	6.3×10^{-4}
number of galaxies	8.9×10^{6}	9.2×10^{6}
FoM	72	80
$\sigma(w_0)$	0.12	0.21
$\sigma(w_a)$	0.41	0.38
$\sigma(\Omega_{\rm DE})$	0.010	0.009
$\sigma(\Omega_k)$	1.9×10^{-3}	1.8×10^{-3}

4 COMBINING WFMOS WITH OTHER DATA SETS

Now we consider the effect of including constraints from other dark energy surveys that will have been undertaken prior to the WFMOS-like survey. We remind the reader that we always include SDSS and Planck data. Not including these data sets while allowing curvature to vary would change the optimal survey – but since that data is available or will soon be, we would end up with a sub-optimal survey. An important question is then whether other planned surveys could also have a strong impact on the optimisation.

Here we consider a generic stage III type-Ia Supernovae survey similar to that outlined in the DETF report (Albrecht et al. 2009), a BAO survey similar to that expected to be completed by WiggleZ (Blake et al. 2009), and another BAO survey planned to be undertaken by BOSS (Schlegel, White & Eisenstein 2009a). BOSS will use measurements of the Lyman-alpha forest from quasar spectra to reconstruct the BAO at high redshift ($z = 2.5$). Since this is still somewhat speculative and has not yet been demonstrated, we consider two cases here, one where the QSO contribution is left out, and another where it is included.

In Section 3 we saw that a survey covering the range $0.1 < z < 1.35$ was favoured with a high FoM. The question we ask now is whether the predecessor experiments will provide good enough measurements of these low-redshift regions to drive the preferred redshift range higher.

The optimal survey parameters are shown in Table 7. The survey parameters as a function of FoM is shown in Figure 6, in both the cases without and with the QSO measurement being included (the full results are shown in Figures B3 and B4 in Appendix B).

Firstly we see that the maximum redshift of the low-redshift bin has increased from $z_{\rm low}({\rm max}) = 1.35$ to $z_{\rm low}({\rm max}) \simeq 1.55 - 1.6$. The minimum redshift of the low-redshift bin no longer peaks at the lowest possible value (as we see from Figure 6), and the FoM is independent of its value up to $z = 0.9$. Since the lower redshift range is already covered by these other experiments, time that could have been spent in that range provides equal value if redeployed to $0.9 < z < 1.6$. A high-redshift bin is again not required, as the low-redshift bin (at $0.9 < z < 1.6$) combined with these other experiments is enough to measure the parameters to sufficient accuracy.

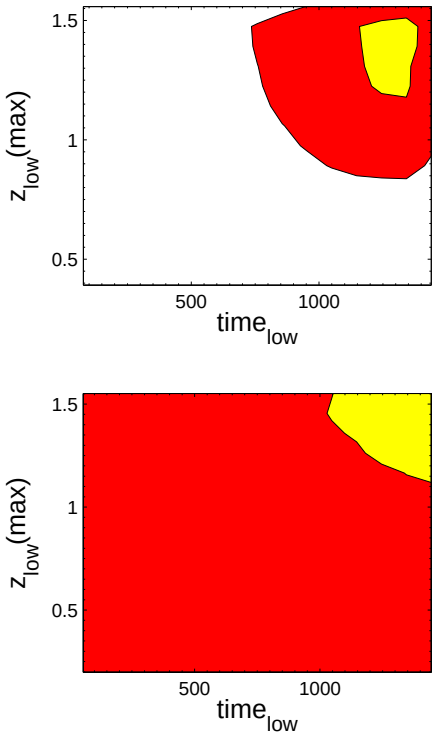

Figure 7. The 60% and 90% flexibility contours for the time and redshift for the low-redshift bin in the case for WFMOS by itself (upper plot), and WFMOS combined with other prior surveys (lower plot). We can see how the flexibility bounds increase when the prior knowledge is stronger and the experiment has less of an impact.

As the extra data sets are included, the flexibility bounds on the survey parameters are expanded. Since the flexibility bounds are given as a percentage of the peak FoM, the survey we are optimizing actually has less of an impact on the total FoM as other data sets are introduced (this is in contrast to parameter estimation, where more data sets normally decrease or 'tighten' the confidence limits on a given parameter). This is very visible in Figure 7, where in the case where the other data sets are added, the 60% flexibility bounds cover most of the possible survey parameter space. Taken to its logical extreme, a survey which adds little or nothing to the state of knowledge will have infinitely large flexibility bounds, as no survey configuration will change the FoM. Such a survey would be obsolete, and there would be little scientific gain in undertaking it. This gives an effective 'window of opportunity' for a WFMOS-like survey, which will still make gains over BOSS, but must be undertaken before a future all-sky dark energy survey (SKA, LSST or JDEM/Euclid), which will have very powerful constraints on the dark energy from a suite of observables (BAO, SN-Ia, weak lensing and cluster number counts).

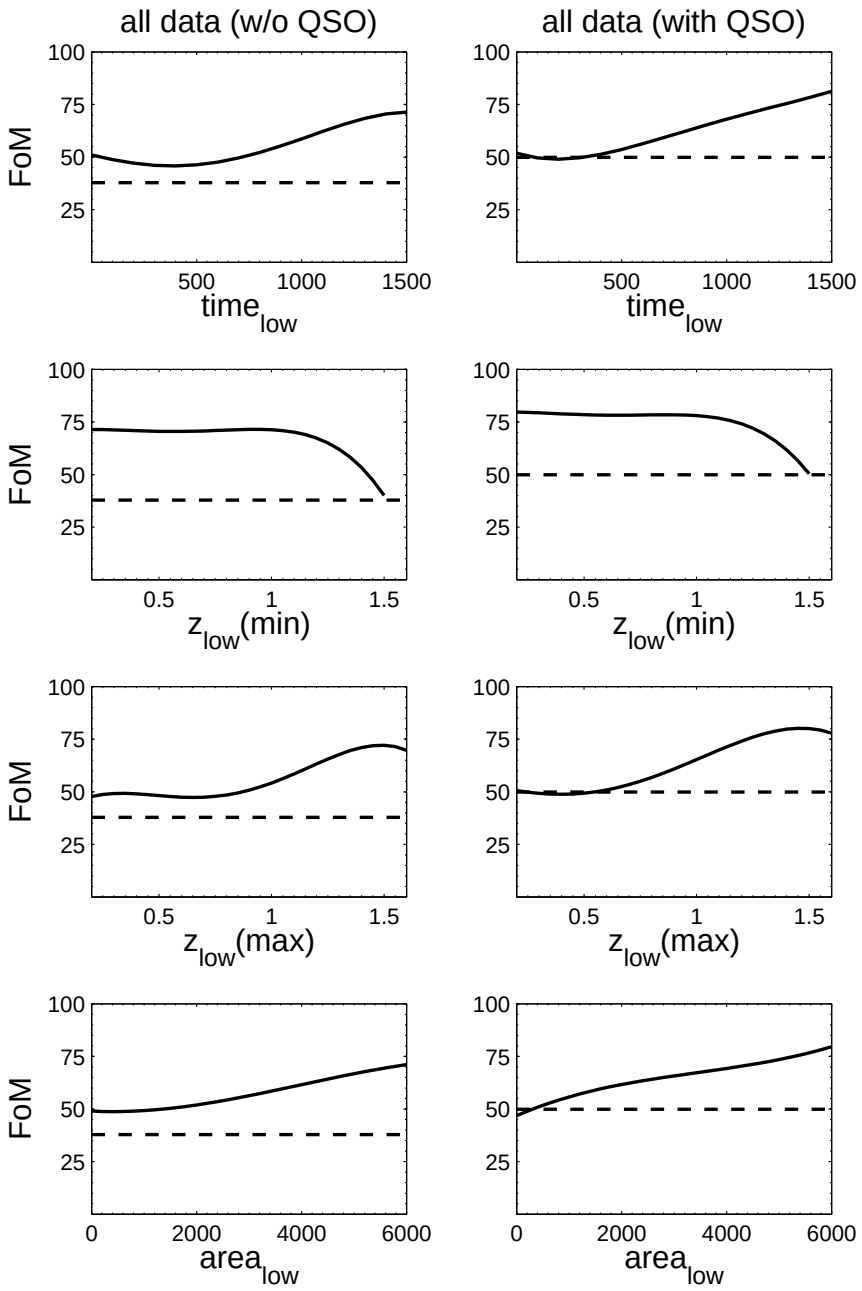

Figure 6. The FoM as a function of the survey parameters when other experiments are included as prior information, with the QSO point not included (on the left), and additionally included (on the right). The extra data at low redshift, $z < 1$, moves the optimal WFMOS survey to a higher redshift of $0.9 < z < 1.55$. The dashed lines show the FoM of the other experiments without WFMOS.

We show the FoM and parameter errors predicted for different surveys individually and combined in Table 8.

5 CONCLUSIONS

We performed an analysis of the optimal dark energy survey that could be carried out in a given time period by an experiment similar in design to WFMOS. We estimate the accuracy of the distance measurements that utilize only the oscillatory part of the power spectrum (the 'wiggles'), using the fitting formula of Seo & Eisenstein (2007). Our measure of utility, or FoM, was defined to be proportional to the area of the error ellipse for the CPL parameters of the dark energy equation of state. Our results can be summarized as follows:

- The high-redshift bin always gives negligible benefit, with the optimal surveys spending all the available time observing at low redshift, $z < 1.6$. The $1.6 < z < 2$ region is the redshift desert where observations of star-forming galaxies are impossible, so $z = 1.6$ represents a hard limit on the optimization.
- The survey area is always the maximum possible (6300

Table 8. FoM and parameter errors for the different surveys that we expect to be available when the WFMOS survey takes place (including the prior information from SDSS and Planck for each of them). Taking the existence of these surveys into account can significantly change the optimization results (see text).

Survey	FoM	$\sigma(w_0)$	$\sigma(w_a)$
WiggleZ	1.1	1.1	4.25
SN-Ia (stage III)	3.7	0.46	2.5
BOSS (no-QSO)	6.6	0.47	1.98
BOSS (+ QSO)	21	0.21	0.71
WFMOS	34	0.21	0.64
Combined	80	0.12	0.37

square degrees under our assumptions) with the exposure time per field of view always as close as possible to the minimum allowed (15 minutes, more than enough to obtain spectroscopic redshifts for the majority of line-emission galaxies on an 8-metre class telescope).

- The principal optimization decision to be made is the upper limit of the low-redshift range, with different values favoured depending on the cosmological model assumptions made.
- Assuming a flat universe and no external data (beyond Planck) an upper limit of $z = 0.7$ is sufficient. The introduction of curvature requires the survey to push up to $z = 1.35$ for WFMOS alone.
- The inclusion of external data sets, such as planned Supernovae and BAO surveys whose results may predate the running of a WFMOS-like survey, changes the optimal redshift range. The optimal maximum redshift of the low-redshift bin is moved up to $z = 1.55$. These data make good measurements of the dark energy properties at $z < 1$, the FoM is insensitive to the minimum of the low-redshift bin as long as $z_{\rm low}(\min) < 0.9$.

We find some of our conclusions of the optimal BAO surveys to be comparable to the optimal configurations of other Dark Energy surveys. The maximization of the survey area is the optimal configuration in both Weak Lensing (Yamamoto et al., 2007) and ISW surveys (Douspis, et al., 2008). However, these types of surveys are not so sensitive to the choice of redshift range as BAO surveys.

It would be possible to go beyond the flat ΛCDM model with the dark energy equation of state described by something different to the CPL parameterization. One example would be a form of $w(z)$ that remains constant at early times before undergoing a rapid transition at some redshift to a negative value at late times to drive the acceleration. This parameterization has been studied in a number of publications (Bassett et al. 2002; Corasaniti & Copeland 2003, etc). However, the constraints on the parameters of this parameterization are often non-Gaussian, and so the predicted constraints using a Fisher matrix approach are often incorrect (when checked against a more rigorous analysis using MCMC techniques). While we investigated optimal surveys using this dark energy parameterization, the results proved, using present methodology, to be uncomfortably unreliable.

We also showed that the flexibility bounds on the survey parameters expand as other datasets are added in as prior information. While the flexibility bounds should not be too narrow, as this could lead to fine tuning of the survey which may not be realizable in practice, when the flexibility bounds become too large it is because the instrument is having too small an impact — its contribution to the total science from all surveys up to that point will be negligible. This leaves a 'window of opportunity' for a WFMOS-like survey such that it will be of scientific benefit if it is performed after WiggleZ and BOSS, but will become obsolete if it post-dates a full-sky BAO survey performed by JDEM, Euclid or SKA.

Finally, the conclusion that an optimal WFMOS-like survey should target exclusively $0.1 < z < 1.5$, aiming for the maximal possible area and therefore the shortest possible exposure time allowing for redshift determination, has been shown here to be quite stable. While such a survey returns the maximal information gain on the dynamical dark energy parameters, other science cases could be made for a high redshift bin, such as using redshift space distortions to probe the growth of structure, and so the theory of gravity. The Dark Energy optimal survey would also not be as good for other science goals like galaxy evolution, which desire high signal-to-noise spectra rather than redshifts alone. As we have shown that such deeper exposures are of negligible benefit to the dark energy FoM, an instrument aiming to carry out both types of science would need to do so via separate survey programmes, rather than by sharing of a single dataset.

ACKNOWLEDGMENTS

This research was undertaken as part of the Conceptional Design Phase (CoDR) for the Gemini/Subaru WFMOS instrument and was partly funded via AURA Contract No. 0525280-GEM00467. DP received support under this contract. We are grateful to the WFMOS "team A" for their help and guidance during this CoDR. We acknowledge Andrey Kaliazin for debugging assistance. DP, MK, ARL and RCN are supported by STFC. MV is supported by the Raffy Manoukian Scholarship and partially supported by the Philip Wetton Scholarship at Christ Church, Oxford. The analysis was performed on the Glamdring cluster of Oxford University, the Archimedes computing cluster at the University of Sussex, supported by funds from SRIF3, and the COSMOS supercomputer in Cambridge, supported by SGI, Intel, HEFCE and STFC.

REFERENCES

Albrecht A. J., *et al.*, 2006, astro-ph/0609591
Albrecht A. J., *et al.*, 2009, arXiv:0901.0721 [astro-ph.IM]
Bassett B. A., 2005, Phys. Rev. D, 71, 083517
Bassett B. A., Kunz M., Silk J., Ungarelli C., 2002, MNRAS, 336, 1217
Bassett B. A., Parkinson D., Nichol R. C., 2005a, ApJ, 626, L1
Bassett B. A., Nichol R. C., Eisenstein D. J. [and the WFMOS Feasibility Study Dark Energy Team], 2005b, astro-ph/0510272
Bassett B. A., Fantaye Y., Hlozek R., Kotze J., 2009, arXiv:0906.0993 [astro-ph.CO]. Fisher4Cast matlab toolbox can be found at http://www.cosmology.org.za/
Blake C., Parkinson D., Bassett B. A., Glazebrook K., Kunz M., Nichol R. C., 2006, MNRAS, 365, 255
Blake C. *et al.*, 2009, MNRAS, 395, 240

Cerny V., 1985, J. Opt. Theory Appl., 45:1, 41
Chevallier M., Polarski D., 2001, Int. J. Mod. Phys., D10, 213
Clarkson C., Cortes M., Bassett B. A., 2007, JCAP, 0708, 011
Corasaniti P. S., Copeland E. J., 2003, Phys. Rev. D, 67, 063521
Douspis, M., Castro, P. G., Caprini, C., Aghanim, N., 2008, A&A 485, 395
Eisenstein D. J. *et al.*, 2005, ApJ, 633, 560
Linder E. V., 2003, Phys. Rev. Lett., 90, 091301
Mukherjee P., Kunz M., Parkinson D., Wang Y., 2008, Phys. Rev. D, 78, 083529
Myers A. D., Brunner R. J., Nichol R. C., Richards G. T., Schneider D. P., Bahcall N. A., 2007 ApJ, 658, 85
Parkinson D., Blake C., Kunz M., Bassett B. A., Nichol R. C., Glazebrook K., 2007, MNRAS, 377, 185 [P07]
Percival, W. J., Cole, S., Eisenstein, D. J., Nichol, R. C., Peacock, J. A., Pope, A. C. and Szalay, A, S., 2007 MNRAS, 381, 1053.
Rassat, A. *et al.*, 2008, arXiv:0810.0003 [astro-ph].
Schlegel D., White M., Eisenstein D., [with input from the SDSS-III collaboration], 2009a, arXiv:0902.4680 [astro-ph.CO]
Schlegel D. J., *et al.*, 2009b, arXiv:0904.0468 [astro-ph.CO]
Seo H. J., Eisenstein D. J., 2007, ApJ, 665, 14
Vardanyan M., Trotta R., Silk J., 2009, arXiv:0901.3354 [astro-ph.CO]
Wake D. A., *et al.*, 2008, MNRAS 387, 1045
Wang X., Chen X., Zheng Z., Wu F., Zhang P., Zhao Y., 2009, MNRAS, 394, 1775
Wit E., Nobile A., Khanin R., 2005, J. Roy. Stat. Soc., C54, 817
Wu, H. Y., Rozo, E., Wechsler, R. H., 2009, arXiv:0907.2690 [astro-ph.CO].
Yamamoto, K., Parkinson, D., Hamana, T., Nichol, R. C., Suto, Y., 2007 Phys. Rev. D76, 023504. [Erratum-ibid. 2007, Phys. Rev. D76, 129901]

APPENDIX A: FISHER MATRIX FORMALISM

As in our previous paper (P07), we use a Fisher matrix approach to compute the predicted experimental constraints on the cosmological parameters. The Fisher matrix is defined to be

$$F_{AB} = \frac{\partial^2(-\ln\mathcal{L})}{\partial\theta_A\partial\theta_B}\,, \tag{A1}$$

where $\mathcal{L}$ is the likelihood, and θ_i is one of the cosmological parameters. By the Cramer–Rao bound, the inverse of the Fisher matrix gives an estimator of the smallest (co)variance of the parameters.

In our previous work we computed the Fisher matrix exactly, but considerations of the parameter set being used and the experimental data that could be included meant that in this work we compute the Fisher matrix elements numerically.[4]

We do this by first gathering up all the experimental data that will be considered (the WFMOS survey configuration under consideration, Planck, the SDSS BAO point, plus whatever other datasets we are including), and simulating their observables ($d_{\rm A}$ & $H(z)$ for BAO experiments, R & l_a for Planck, d_l for supernovae experiments) at the fiducial cosmology, with no scatter in the mean values. Since the Fisher matrix is defined as the expectation of the Hessian of the log-likelihood, averaged over all possible realizations of the data, this averaging process removes the scatter in the mean of the data point. Then we use this to compute the likelihood in the region around the fiducial cosmology.

We can compute the slope of a function through a finite-difference operation. For example, the slope of a function f evaluated at x can be given by

$$f'(x) = \frac{f(x+\epsilon) - f(x-\epsilon)}{2\epsilon}\,, \tag{A2}$$

where ϵ is some small positive number. As we are evaluating the likelihood at the fiducial cosmology, which should be identical to the maximum likelihood point, the slope of the likelihood in any direction should be zero, or as close to it as numerical accuracy will allow. Here we use the finite-difference method to compute the second derivative of the likelihood, evaluated at the fiducial cosmology.

For each individual Fisher matrix element we take steps of size ϵ in both cosmological parameters. We can estimate the slope in the direction of one of the parameters at the displaced point of the other, i.e.

$$\frac{\partial(-\ln\mathcal{L}(\theta_B \pm \epsilon))}{\partial\theta_A} = -\frac{\ln\mathcal{L}(\theta_B \pm \epsilon, \theta_A + \epsilon) - \ln\mathcal{L}(\theta_B \pm \epsilon, \theta_A - \epsilon)}{2\epsilon}\,. \tag{A3}$$

(This holds also if θ_A and θ_B are exchanged.) From here our estimate of the second derivative is simply the finite difference of the slopes, evaluated at the slightly displaced positions,

$$\frac{\partial^2(-\ln\mathcal{L})}{\partial\theta_A\partial\theta_B} = \frac{1}{2\epsilon}\left[\frac{\partial(-\ln\mathcal{L}(\theta_B+\epsilon))}{\partial\theta_A} - \frac{\partial(-\ln\mathcal{L}(\theta_B-\epsilon))}{\partial\theta_A}\right]. \tag{A4}$$

We tune the step parameters ϵ to be small enough to achieve numerical convergence of the Fisher matrix.

APPENDIX B: FULL PRESENTATION OF RESULTS

[4] Similar work by Bassett et al. (2009) has made such numerical computation available as a MATLAB toolbox (called Fisher4Cast), available at http://www.cosmology.org.za/

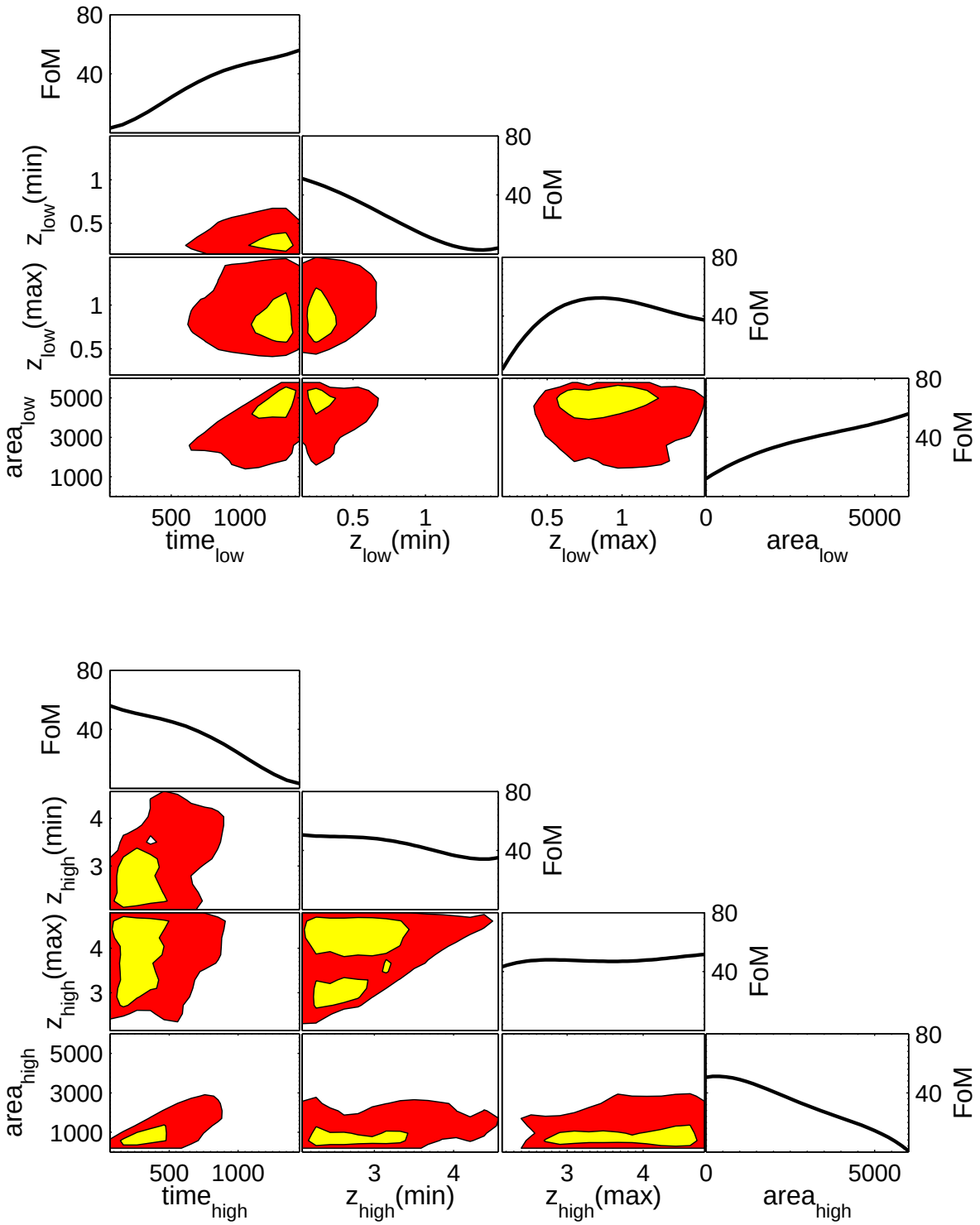

Figure B1. The optimal FoM as a function of the survey parameters (where the other parameters are chosen to maximize the FoM), for surveys optimized for a flat universe. The 2-d contours delimit the 90% and 60% flexibility bounds. We see the optimal survey is one that spends all its time at low redshift ($\text{time}_{\text{low}} = 1500$hrs) and maximizes the area in the low-redshift bin. We see that the high-redshift bin adds nothing to the FoM, and so it is insensitive to those parameters, except the time in the high-redshift bin which is minimized.

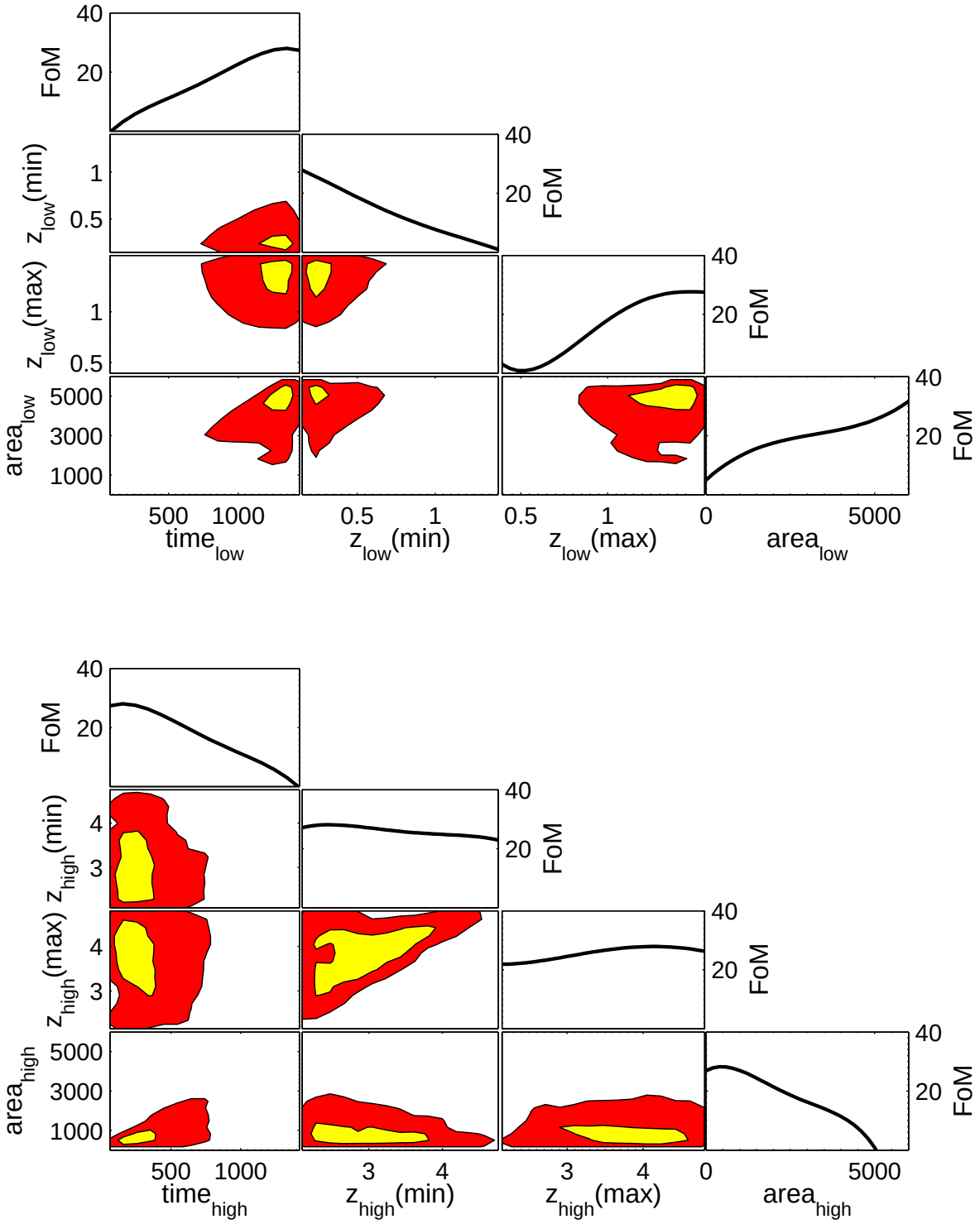

Figure B2. The FoM as a function of the survey parameters (where the other parameters are chosen to maximize the FoM), for surveys optimized including curvature as a nuisance parameter. The 2-d contours delimit the 90% and 60% flexibility bounds. We see the optimal survey is one that spends all its time at low redshift and maximizes the area in the low-redshift bin, but now the optimal maximum of the low-redshift bin is moved up to $z = 1.35$. As before, we see that the high-redshift bin adds nothing to the FoM, and so it is insensitive to those parameters, except the time in the high-redshift bin which is minimized.

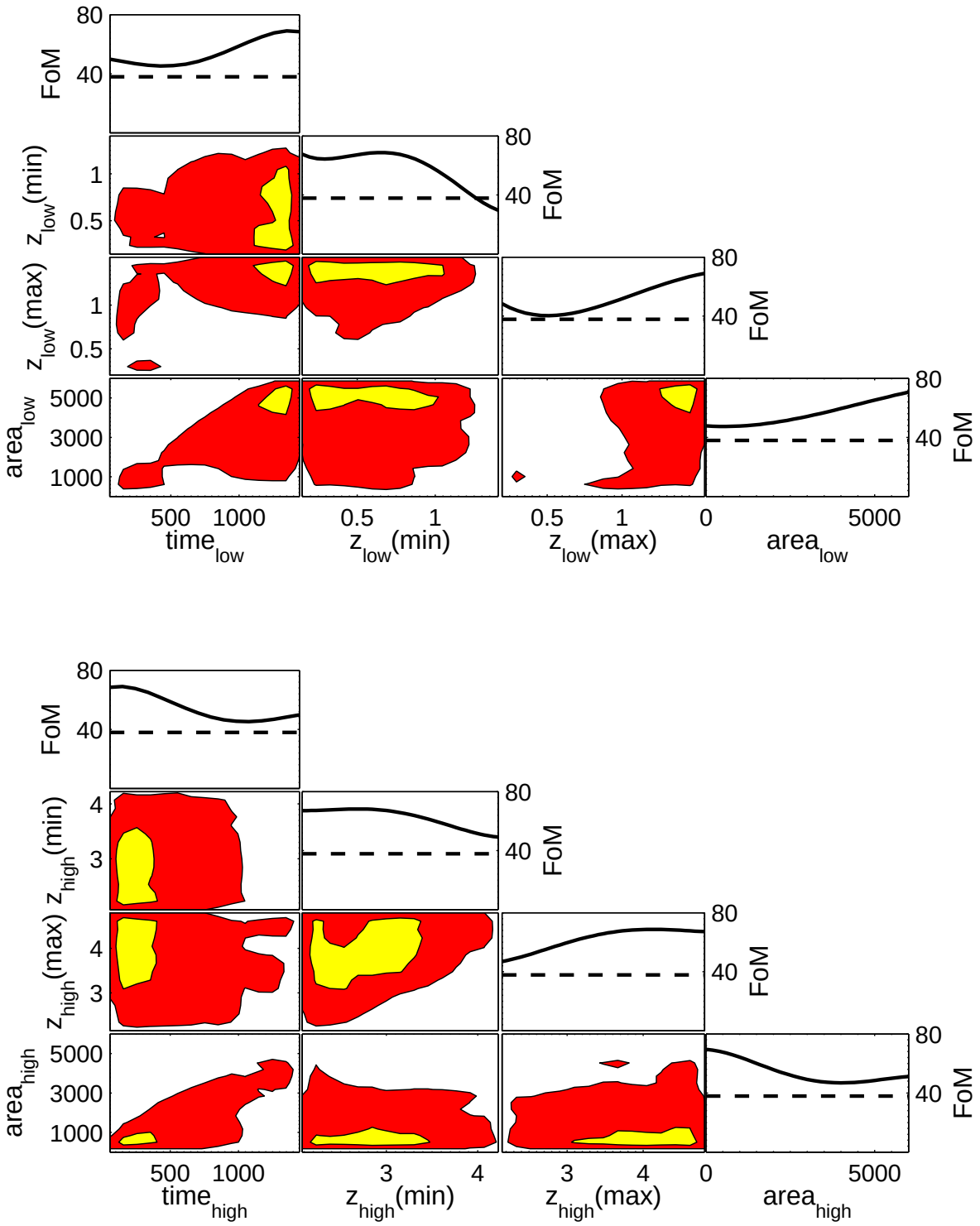

Figure B3. The FoM as a function of the survey parameters for a WFMOS-like survey with other data sets (SN-Ia, BOSS, but without the QSO point at z=2.5, and WiggleZ) included as external datasets. The dashed line shows the FoM of the other surveys combined (including Planck), but without WFMOS. The 2-d contours delimit the 90% and 60% flexibility bounds. We see the optimal survey is one that spends all its time at low redshift and maximizes the area in the low-redshift bin. The FoM now peaks at $z = 1.55$ for the maximum of the low-redshift bin, but is insensitive to the minimum as long as $z_{\rm low}(\rm min) \leq 0.9$. As before, we see that the high-redshift bin adds nothing to the FoM, and so it is insensitive to those parameters, except the time in the high-redshift bin which is minimized.

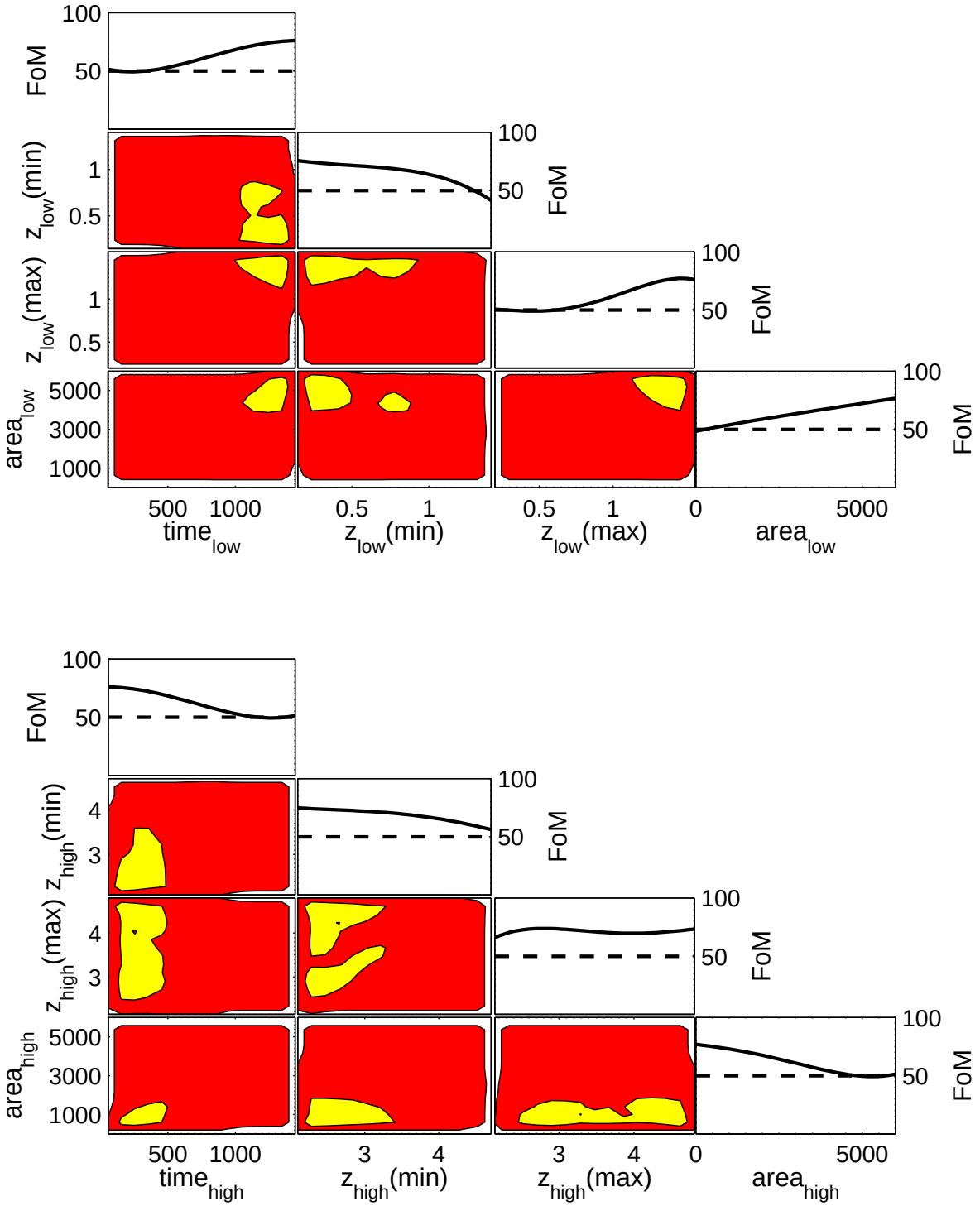

Figure B4. The FoM as a function of the survey parameters for a WFMOS-like survey with other data sets (SN-Ia, BOSS with the QSO point at z=2.5 and WiggleZ) included as external datasets. The dashed line shows the FoM of the other surveys combined (including Planck), but without WFMOS. The 2-d contours delimit the 90% and 60% flexibility bounds. We see the optimal survey is one that spends all its time at low redshift and maximizes the area in the low-redshift bin. The FoM now peaks at $z = 1.6$ for the maximum of the low-redshift bin, but is insensitive to the minimum as long as $z_{\rm low}(\min) \leq 0.9$. Notice that the 60% flexibility bound now covers most of the survey parameter space.